Nanoelectronics and Its New Materials – A NEW ERA OF NANOSCIENCE

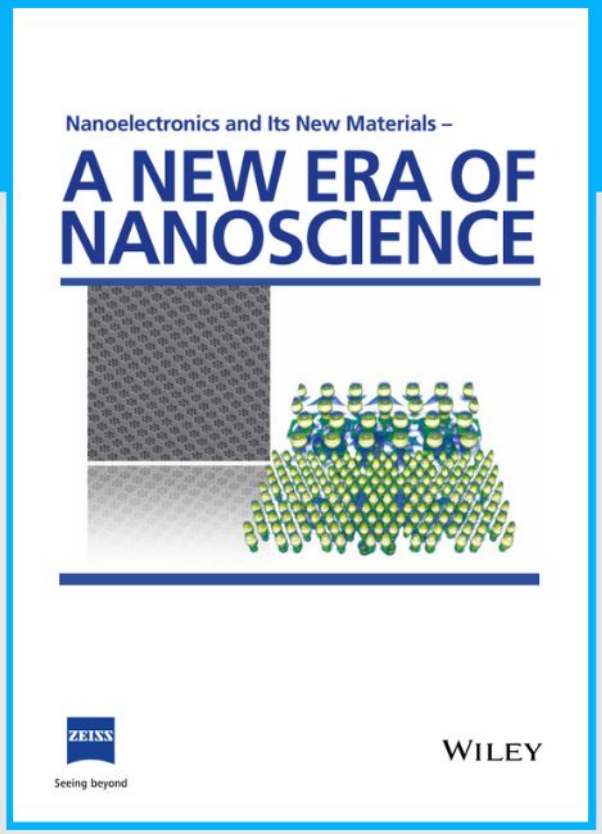

Discover the recent advances in electronics research and fundamental nanoscience.

Nanotechnology has become the driving force behind breakthroughs in engineering, materials science, physics, chemistry, and biological sciences. In this compendium, we delve into a wide range of novel applications that highlight recent advances in electronics research and fundamental nanoscience. From surface analysis and defect detection to tailored optical functionality and transparent nanowire electrodes, this eBook covers key topics that will revolutionize the future of electronics.

To get your hands on this valuable resource and unleash the power of nanotechnology, simply download the eBook now. Stay ahead of the curve and embrace the future of electronics with nanoscience as your guide.

ZEISS

Seeing beyond

WILEY

NANO · MICRO small
www.small-journal.com

Investigation of the Photocatalytic Hydrogen Production of Semiconductor Nanocrystal-Based Hydrogels

*Jakob Schlenkrich, Franziska Lübkemann-Warwas, Rebecca T. Graf, Christoph Wesemann, Larissa Schoske, Marina Rosebrock, Karen D. J. Hindricks, Peter Behrens, Detlef W. Bahnemann, Dirk Dorfs, and Nadja C. Bigall**

Destabilization of a ligand-stabilized semiconductor nanocrystal solution with an oxidizing agent can lead to a macroscopic highly porous self-supporting nanocrystal network entitled hydrogel, with good accessibility to the surface. The previously reported charge carrier delocalization beyond a single nanocrystal building block in such gels can extend the charge carrier mobility and make a photocatalytic reaction more probable. The synthesis of ligand-stabilized nanocrystals with specific physicochemical properties is possible, thanks to the advances in colloid chemistry made in the last decades. Combining the properties of these nanocrystals with the advantages of nanocrystal-based hydrogels will lead to novel materials with optimized photocatalytic properties. This work demonstrates that CdSe quantum dots, CdS nanorods, and CdSe/CdS dot-in-rod-shaped nanorods as nanocrystal-based hydrogels can exhibit a much higher hydrogen production rate compared to their ligand-stabilized nanocrystal solutions. The gel synthesis through controlled destabilization by ligand oxidation preserves the high surface-to-volume ratio, ensures the accessible surface area even in hole-trapping solutions and facilitates photocatalytic hydrogen production without a co-catalyst. Especially with such self-supporting networks of nanocrystals, the problem of colloidal (in)stability in photocatalysis is circumvented. X-ray photoelectron spectroscopy and photoelectrochemical measurements reveal the advantageous properties of the 3D networks for application in photocatalytic hydrogen production.

1. Introduction

One of the main challenges in recent decades is the transformation toward a sustainable energy system.[1] Hydrogen is a widely discussed alternative to fossil fuels and besides the yet industrially applied electrolysis, photocatalytic hydrogen production could be a method to supply hydrogen. A variety of materials, for example, TiO_2, MoS_2, CdS, SiC, or g-C_3N_4, has been investigated to find a suitable candidate to use sunlight efficiently for photocatalytic hydrogen production.[2–4] In addition to the type of material, the structure or morphology plays a crucial role in the design of the catalyst.[5] Nanomaterials in general provide a large surface-to-volume ratio leading to a high amount of catalytically active surface in an overall low amount of material. The expertise in the field of solution-based nanocrystal (NC) synthesis acquired over the past decades enables the production of a large number of different NC with a variety of shapes.[6–10] Especially, CdSe, CdS, and CdSe/CdS

J. Schlenkrich, F. Lübkemann-Warwas, R. T. Graf, C. Wesemann, L. Schoske, M. Rosebrock
Leibniz University Hannover
Institute of Physical Chemistry and Electrochemistry
Callinstraße 3A, 30167 Hannover, Germany

F. Lübkemann-Warwas, L. Schoske, M. Rosebrock, K. D. J. Hindricks, P. Behrens, D. Dorfs, N. C. Bigall
Cluster of Excellence PhoenixD (Photonics Optics and Engineering -Innovation Across Disciplines)
Leibniz University Hannover
30167 Hannover, Germany
E-mail: nadja.bigall@pci.uni-hannover.de

The ORCID identification number(s) for the author(s) of this article can be found under https://doi.org/10.1002/smll.202208108.

DOI: 10.1002/smll.202208108

R. T. Graf, P. Behrens, D. Dorfs, N. C. Bigall
Laboratory of Nano- and Quantum Engineering
Leibniz University Hannover
30167 Hannover, Germany

K. D. J. Hindricks, P. Behrens
Leibniz University Hannover
Institute of Inorganic Chemistry
Callinstraße 9, 30167 Hannover, Germany

D. W. Bahnemann
Leibniz University Hannover
Institute of Technical Chemistry
Callinstraße 5, 30167 Hannover, Germany

D. W. Bahnemann
Laboratory "Photoactive Nanocomposite Materials"
Saint-Petersburg State University
Ulyanovskaya str. 1, Saint-Petersburg, 198504 Peterhof, Russia

heterostructured NCs have been intensively studied and the synthetic control of these materials allows specific design for the targeted application.[10–14] Therefore, of particular interest is the design of the NC heterostructure, which allows targeted influence on the charge carrier mobility, its residence probability as well as band structure. Compared to the band structure of the pure CdSe quantum dots (QD) and CdS nanorods (NRs), with band gap energies of 1.7 and 2.4 eV, respectively, the CdSe/CdS dot-in-rod NR exhibits a quasi-type-II electronic structure. Here, the band offset of the conduction bands is small enough to allow the electron to delocalize over the entire NRs, whereas the hole is localized in the core (**Figure 1**). For photocatalytic applications, the choice of band structure in the semiconductor material is the first important step, but it has already been shown that pure semiconductor NCs are not as efficient as they are estimated to be.[15–17] Therefore, a metal-based co-catalyst is usually added to capture the sunlight in the semiconductor and transfer the excited electrons from the semiconductor to the co-catalyst where the catalytic hydrogen production takes place. Metal complex[18] can be used as co-catalysts or a metal-based co-catalyst domain, for example, Pt, Au, Au—Pt, Ni, and many more,[15,19–21] can be grown on the semiconductor to obtain an efficient photocatalyst. When using ligand-stabilized NCs as photocatalysts the ligand surface has a major impact on the overall efficiency.[22–24] Some ligands, for example, mercaptopropionic acid (MPA), can lead to trap states which have an influence on the charge carrier dynamics and lifetimes.[22] Others are sterically large in size and therefore have an influence on the catalytic behavior. Generally, the accessibility of the catalytic surface, the lifetime of the charge carrier, and the stability of the NCs play a key role in the efficiency of the photocatalytic reaction. The accessibility of the surface can be influenced on the one hand by the stabilizing ligand shell (too much prevent access to the surface) and on the other hand by the stability of the NCs in solution. If the NCs agglomerate in a way that the accessible surface area is reduced, the photocatalytic efficiency decreases.

In addition to the properties already discussed, the morphology of the photocatalyst may also influence the resulting efficiency and make the material interesting for future applications. A novel class of materials with an interesting morphology are nanocrystal-based gel structures, which exhibit high porosity and combine physicochemical properties of the NCs with the size of bulk material.[25–28] Nanocrystal-based gel structures undergo a controlled destabilization of the ligand-stabilized nanocrystal solution to form a 3D, highly porous network which retains the properties of the NC building blocks. As has already been shown, semiconductor NC-based networks, for example, CdSe,[29] CdS,[30] and CdSe/CdS,[31–33] can even exhibit improved and novel properties compared to the NCs in solution. A prominent feature of semiconductor NC-based gel structure is their electron and hole wavefunction beyond one single NC, which results from the crystal-to-crystal bond of the individual NC building blocks (Figure 1). In gel structures consisting of only one semiconductor material, for example, CdSe or CdS, this can lead to a delocalization of the charge carriers

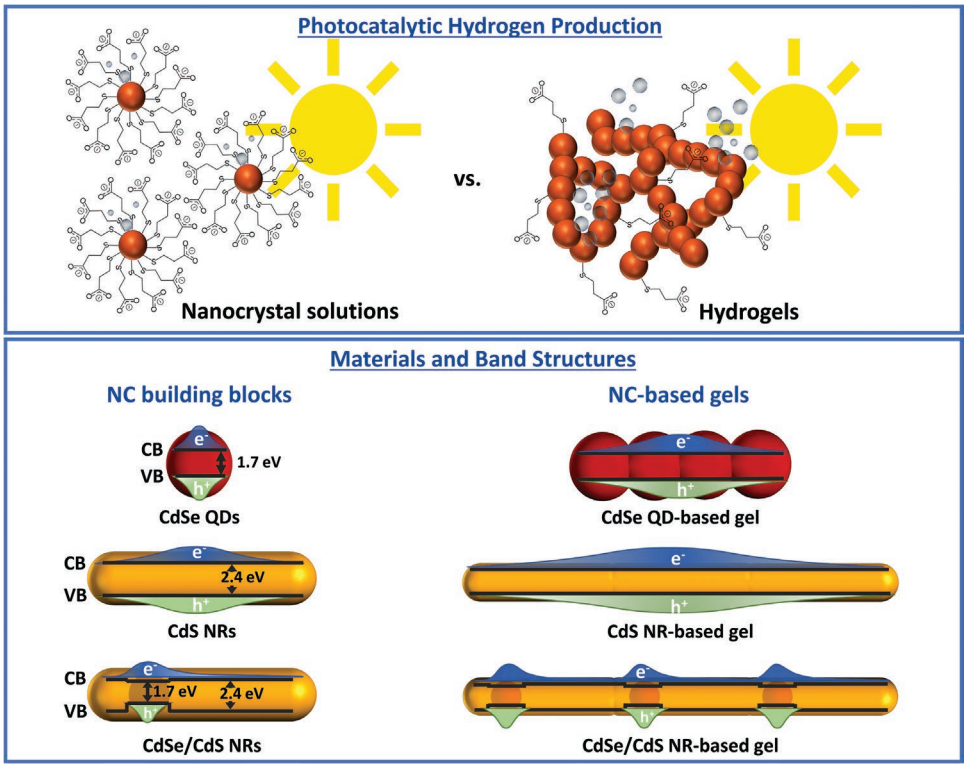

Figure 1. Schematic illustration of the photocatalytic hydrogen production combined with the materials and band structures of the NC building blocks and NC-based gels used (symbolized as a chain of three and four nanocrystals in direct contact). After a phase transfer from organic to an aqueous solution, the ligand-stabilized nanocrystals are destabilized by ligand oxidation with H_2O_2. Nanocrystals in aqueous solution and hydrogels can be used for photocatalytic hydrogen production.

beyond one NC which would have a minor effect on the charge carrier separation in these network structures. However, the charge carrier separation in gel structures consisting of a semiconductor heterostructure, for example, CdSe/CdS, is significantly increased by the quasi-type-II electronic structure. In previous work, optical and photoelectrochemical investigations of CdSe/CdS NR-based gel structures have shown that crystal-to-crystal contact leads to a significant increase in charge carrier lifetime as well as charge carrier mobility and charge carrier separation. The long-lived charge carrier separation improves reactions of the respective charge carriers on the surface of the gel network.[31–34] Semiconductor NC-based gel networks combine the advantages of pure NC, such as high control of electronical properties through synthesis, as well as high surface-to-volume ratio, and the advantages of a gel structure, for example, a high porosity, easily accessible surface, increased probability of charge carrier separation through crystal-to-crystal contact, in one material. Thus, all advantages make the gel structures to a promising class of materials for application in photocatalysis.[35]

In this work, we present the influence of gel network formation of different semiconductor NC building blocks, here CdSe QDs, CdS NRs, and CdSe/CdS dot-in-rod-shaped NRs, on photocatalytic hydrogen production in aqueous solutions in comparison to their non-gelated NC building block counterparts (Figure 1). To destabilize the ligand-stabilized NC solutions, an oxidative method using H_2O_2 was used. Removal of the ligands from the surface leads to the formation of a hydrogel with more freely accessible surface and different surface properties, such as the formation of sulfate sites, compared to the ligand-stabilized NCs. In addition to the influence of gel network formation and band structure of the various NC building blocks, the influence of different hole scavengers, for example, methanol (MeOH), triethanolamine (TEOA), ascorbic acid (Ascorb.), and a mixture of sodium sulfide and sodium sulfite (Na_2S/Na_2SO_3), on the photocatalytic hydrogen production is shown. Furthermore, the CdSe/CdS system was investigated for its long-term stability due to its special quasi-type II band structure and high photocatalytic hydrogen production as a model system. X-ray photoelectron spectroscopy (XPS) and intensity-modulated photocurrent spectroscopy (IMPS) are used to obtain information on the mechanistic reactions and the differences between NC-based gel structure and non-gelated NCs. The assembly and immobilization of NCs into highly porous and voluminous NC-based gel networks significantly increase hydrogen production while enabling a better applicability of the functional NCs.

2. Results and Discussion

2.1. Structural and Optical Properties of Nanocrystal-Based Gel Structures

CdSe QD-, CdS NR-, and CdSe/CdS NR-based hydrogels have been synthesized by the addition of a 0.35 wt% H_2O_2 solution to a mercaptopropionic acid-stabilized NC solution. The oxidizing agent partially removes the thiolate ligands (RS^-) by forming radicals (RS•), allowing controlled destabilization of the nanocrystal solution and the controlled assembly into a porous hydrogel.[30] After the gel formation, the solvent must be replaced to remove residual oxidation agent and oxidized and detached ligands. With this method partially transparent and slightly turbid hydrogels were obtained, which still possess the volume of the NC solutions (**Figure 2**).

Scanning electron microscope (SEM) images of supercritically dried hydrogels (aerogels) were obtained to further visualize the structure and porosity of the NC-based aerogels (Figure 2, center images). From the SEM images, a highly porous and voluminous network structure can be seen, which is comparable to that in hydrogels. However, it can be assumed that due to the supercritical drying process and the associated solvent exchange from water to acetone to liquid CO_2, there is a slight shrinkage of the aerogels, so that most likely a more filigree and slightly more porous structure is present in the hydrogel. To get a rough estimation of the specific surface area, Brunauer–Emmet–Teller nitrogen physisorption measurements (BET)[36] of the aerogels were performed (Figure S3, Supporting Information). All three semiconductor aerogels have a specific surface area of 160–200 $m^2\ g^{-1}$.

Further insights in the interconnection between the NC building blocks are shown in the transmission electron microscope (TEM) images (Figure 2, right images) prepared from hydrogels after several washing steps. For all three different types of semiconductor NCs, the TEM images show that the NC building blocks are interconnected by a direct crystal-to-crystal contact with grain boundaries in between two different nanocrystals (Figure S1, Supporting Information). In case of the CdS NRs and CdSe/CdS NRs, the building blocks are preferentially connected tip-to-tip or tip-to-side and only to a minor extend side-to-side. This behavior is typical for NR-based gel structures, as shown in previous work by our group.[31,33,37,38]

The optical properties of the hydrogels are very similar to those of the NC solutions showing that the nanoscopic properties are retained in the macroscopic gel networks. However, differences can be observed in the photoluminescence (PL) properties (e.g., PL lifetimes, PL quantum yield (QY)). These properties have been studied intensively in previous works of our group and are discussed in detail in the Supporting Information (Figure S2, Supporting Information). Here we want to highlight the changes in the PL lifetimes from NCs in solution to hydrogels. In all types of hydrogels, a long lifetime component additionally to the short lifetime component of the NCs can be observed.[31] Due to the interconnection of the individual NCs, the excited electrons can be delocalized beyond one NC building block. In the CdSe QD-based and CdS NR-based hydrogels, the excited hole can likely also be delocalized, while in CdSe/CdS NRs due to the quasi-type-II band structure the hole is preferably located in the CdSe core. The possible delocalization of excited electrons in the network and localization of the hole in the CdSe core effectively separate the charge carriers, which reduces the overlap of the electron and hole wave functions and increases the charge carrier lifetimes.[39] The network formation thus has an impact on the charge carrier properties and is likely to be the reason why the photocatalytic properties are higher in these systems, as will be demonstrated below.

To further investigate the charge carrier dynamics transient absorption (TA) measurements would be very interesting. We ourself have not yet been able to measure the hydrogels in a TA.

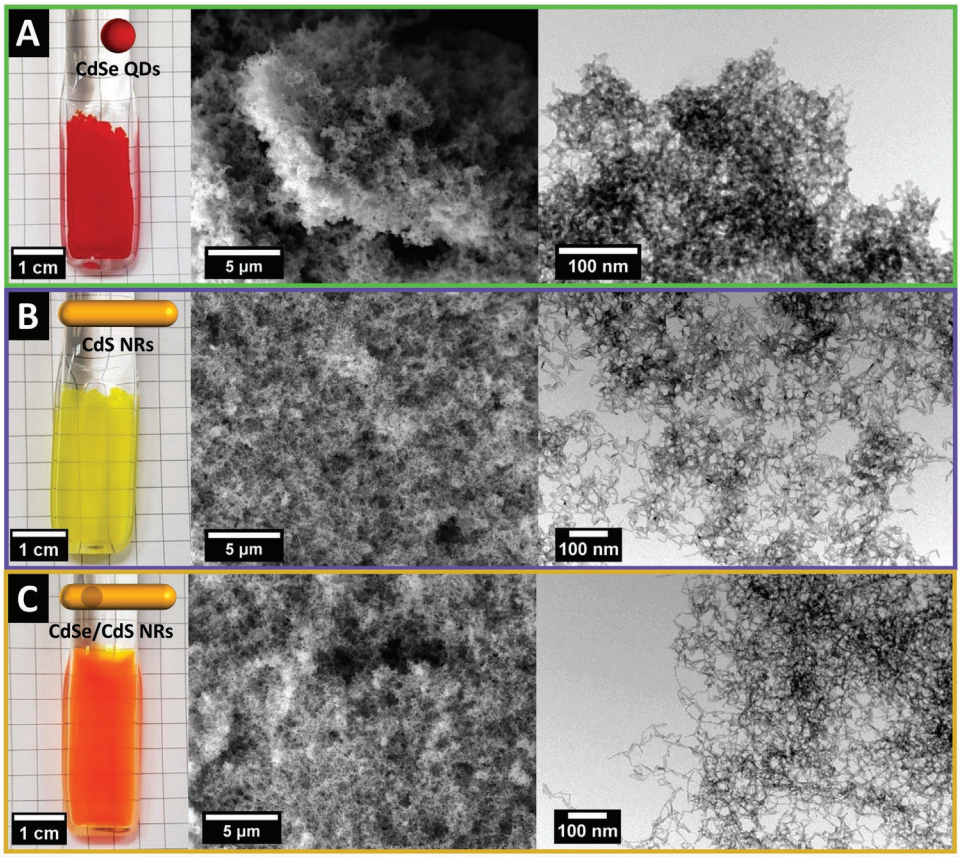

Figure 2. Structural visualization of the 3D networks of A) CdSe QD, B) CdS NR, and C) CdSe/CdS NR-based gel structures using (from left) a photograph of a hydrogel, a SEM image of a supercritically dried aerogel and a TEM image prepared from a hydrogel dried on the TEM grid.

Using TA studies from the literature to explain the mechanistic differences of NCs in solution and hydrogels would not be sufficient in our opinion. As Micheel et al.[22] and Berr et al.[40] showed in their studies, the hole and electron trap states have a major impact on the resulting TA measurements. Since we change the trap state situation in the hydrogels by removing the thiol ligands, we would expect a different TA signal compared to most ligand-stabilized nanoparticle systems. Additionally, most TA studies of CdS/CdS NR were performed without a hole scavenger. As well shown by Berr et al.[40] this again affects the results from the TA measurements. To discuss the charge carrier dynamics in detail, TA measurements with the hydrogels and the hole scavenger should be performed.

2.2. Photocatalytic Properties of NC Solutions and NC-Based Hydrogels

NC-based hydrogels have a self-supporting 3D structure with water inside the pore system. By exchanging the water with an aqueous solution of a hole scavenger, these hydrogels can be used for photocatalytic experiments. Therefore, the hydrogels were washed five times with the aqueous hole scavenger solutions over 24 h to exchange the medium inside the hydrogel. Due to the self-supporting porous 3D structure, stirring during the experiments is not necessary to ensure a homogeneous solution, as it is usually the case when NCs are used in photocatalytic reactions.[41,42] This is not least due to the low colloidal stability of the ligand-stabilized NCs in the hole scavenger solution. Mercaptopropionic acid (MPA) stabilized NCs are stable only in the 10 vol % MeOH and TEOA solutions and not in ascorbic acid and Na_2S/Na_2SO_3 solutions as demonstrated in Figure S4, Supporting Information, by photographs and dynamic light scattering (DLS) measurements. To quantify the hydrogen production, we assume that the entire semiconductor hydrogel is excited and takes part in the photocatalytic hydrogen production. Due to the higher optical density compared to NC solutions and to ensure complete excitation of the hydrogels, the measurement cells are maximum 2 mm thick, so that the resulting hydrogels are also maximum 2 mm thick (Figure S6, Supporting Information).

All photocatalytic studies were performed for 24 h on the three semiconductor systems on both the pure NC solutions and the hydrogels with four different hole scavenger solutions. Using CdSe and CdS as catalyst materials necessarily leads to the use of a hole scavenger to enable the redox reaction,[43] because the energy levels of the valence bands are not suitable to achieve the oxygen production and thus the full water splitting. It is already known for pure NC solutions that the hole scavenger can have an influence on the hydrogen production.[44,45] So, in this work the four commonly known hole scavengers MeOH, TEOA, ascorbic acid, and sulfide/sulfite (Na_2S/Na_2SO_3)

were applied to the systems. Prior to the photocatalytic experiments, the hydrogels had a monolithic structure that had the volume of the NC solutions used. During the hydrogen production, the monolithic structure slightly broke due to the evolution of gas bubbles which had to rise through the gel network. Thus, corridors were formed where the gas could rise through the gel network (Figure S5, Supporting Information). Interestingly, the photocatalytic experiments in all three semiconductor systems with Na_2S/Na_2SO_3 as hole scavenger show that the hydrogels exhibit a hydrogen production rate several times higher than the corresponding ligand-stabilized NC solutions (**Figure 3**). More specifically, CdSe hydrogels had a 5.75 ± 0.05-fold, CdS hydrogels a 4.72 ± 0.29-fold, and CdSe/CdS hydrogels a 4.61 ± 0.3-fold higher hydrogen production rate than the corresponding non-gelated, ligand-stabilized NC solutions. The use of methanol or triethanol amine as hole scavengers leads to negligible hydrogen production in case of CdSe QDs and CdSe/CdS NRs, whereas the CdS NRs show non-negligible hydrogen production in these hole scavenger solutions. Moreover, it can be overserved in the CdS NR system that the pure NC solutions show higher hydrogen production than the hydrogel in case of MeOH, TEOA, and ascorbic acid, while the hydrogen production is generally low for both the colloid and the gels. The use of ascorbic acid as hole scavenger shows nearly similar hydrogen production rate as the Na_2S/Na_2SO_3 system only in the CdSe QD-based system. The various observations for the different semiconductors in the different hole scavenger solutions could be due to a variety of reasons. As discussed by Schneider et al. the mechanisms of the hole scavenger reactions are complex and it is not trivial to name the reactions that take place.[44] An important key role has the energy level of the electron in the hole scavengers as shown by Berr et al. who observed that the higher the hydrogen production efficiency in CdS/Pt nanoparticle solutions, the stronger the reduction power of the hole scavenger is.[45] The results shown here are not completely in line with the reduction power of the hole scavengers but the general tendency is in good agreement with the results reported by Berr et al. This might be explained by the facts that Berr et al. used pure CdS NR with a Pt domain and all of the hole scavenger molecules form highly reducing free radical intermediates following their one-electron oxidation. These free radicals usually are much more powerful reductants than the original hole scavengers and are known to even inject electrons into the semiconductor's conduction band.[44] This so-called current-doubling phenomenon will in turn explain the increased H_2 formation rates. Beside the current-doubling phenomenon the stability of the intermediate radical can have an influence on the resulting hole scavenging efficiency. Depending on the pH, the free electron in the ascorbic acid radical, for example, can be partially delocalized within the molecule. The back reaction to the ascorbic acid is concurring with a second oxidation step toward a stable product. Thus, the faster the second oxidation step occurs, the less probable the back reaction takes place and the more stable the radical is, the more probable the second oxidation step becomes.

As another argument which does not directly relate to the two oxidation steps, the adsorption ability of the hole scavengers on the semiconductor surface should have an influence. Since the electron transfer from the hole scavenger to the

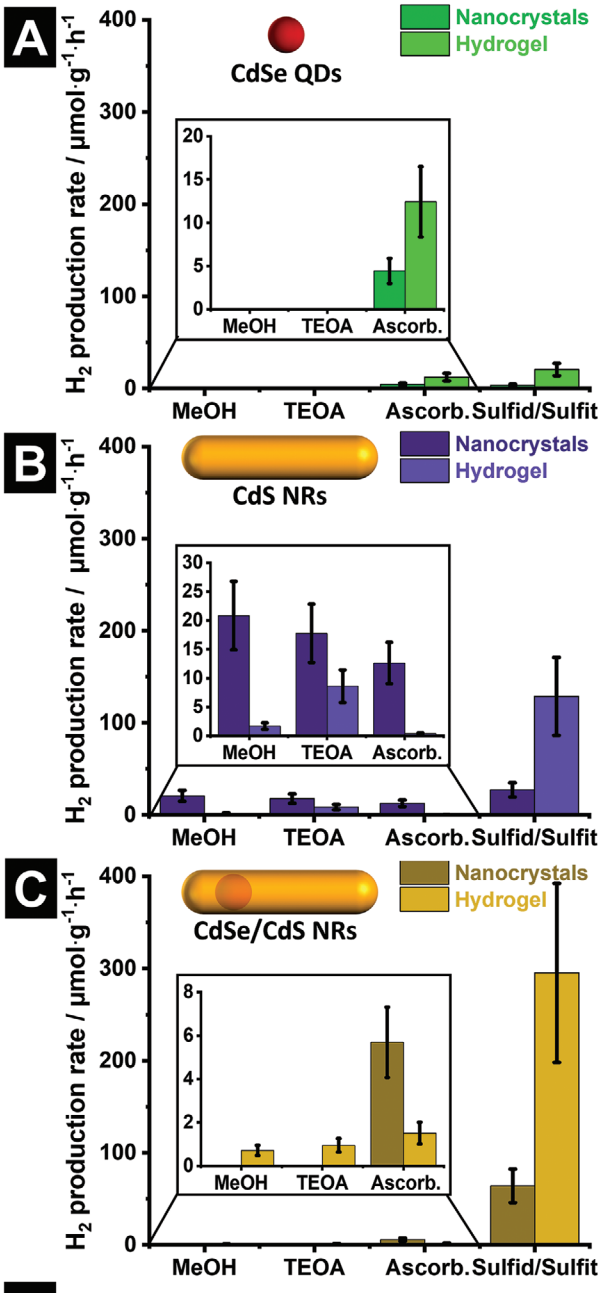

D Apparent quantum efficiencies (AQY) of hydrogels in %

	MeOH	TEOA	Ascorb.	S^{2-}/SO_3^{2-}
CdSe	-	-	0.006	0.01
CdS	0.001	0.008	0.0003	0.11
CdSe/CdS	0.0004	0.0004	0.001	0.16

Figure 3. Photocatalytic hydrogen production of pure NC solutions (dark color) and hydrogels (light color) of A) CdSe QDs, B) CdS NRs, and C) CdSe/CdS NRs with methanol (MeOH), triethanol amine (TEOA), ascorbic acid, and sulfide/sulfite (Na_2S/Na_2SO_3) solutions as hole scavengers measured after 24 h. D) Calculated apparent quantum efficiencies (AQY) of the hydrogels in the different hole scavenger solutions.

semiconductor is more efficient when the molecule or ion is in direct contact with the surface of the semiconductor. A higher adsorption ability would support the opposite to the above discussed two oxidation steps in the case of ascorbic acid. However, it might be very different for the different hole scavengers. For the 0.1 M Na_2S/Na_2SO_3 solution, the stabilization of the radical for the two oxidation steps would not be crucial but here the absorption ability on the surface might play a major role. For ascorbic acid, this could be the opposite.

In particular, for the pure NCs in solution, steric hindrance by the ligand shell has an impact on the surface accessibility of the organic hole scavengers. Furthermore, charge carrier localization and thus surface trap states and especially hole trap states could play a key role in the hole scavenging process, which is discussed in the following for CdS hydrogels.[22] Trap state emission was observed in the emission spectrum of the CdS NCs in solution, which exhibits higher intensity compared to the band gap emission (Figure S2, Supporting Information). This indicates that holes are trapped very efficiently, which could favor the hole scavenging process with the organic hole scavengers MeOH, TEOA, and ascorbic acid. The trapped hole has a longer lifetime and since it is located on the surface it can be extracted from the semiconductor more easily.

The other general observation that a mixture of a 0.1 M Na_2S/Na_2SO_3 solution is the most efficient hole scavenger for the CdSe, CdS, and CdSe/CdS systems is consistent with the findings in literature for different CdS-based NC solutions.[15,45] It has to be emphasized that for all semiconductor systems investigated, a five times higher photocatalytic efficiency of the hydrogels compared to the respective nanocrystal solutions was demonstrated when using a mixture of Na_2S/Na_2SO_3 as hole scavengers. The apparent quantum efficiency (AQY) under illumination with a solar simulator has been determined for all hydrogel samples and is shown in the table Figure 3D. The highest AQY of 0.16% was calculated for the CdSe/CdS NR-based hydrogel with a 0.1 M Na_2S/Na_2SO_3 solution, followed by CdS NR-based hydrogel with 0.11% with a 0.1 M Na_2S/Na_2SO_3 solution. Since photocatalytic studies on NC solutions are often performed in the literature under stirring and excitation with a 455 nm LED,[47] the AQY was also determined here for comparison in addition to the xenon lamp with an AM1.5G filter under stirring using a 455 nm LED for excitation on the CdSe/CdS gel structure (Table S1, Supporting Information). Stirring only slightly increases the AQY by 0.01% for the CdSe/CdS NR-based hydrogels, whereas an increase of 0.09% is seen using excitation with the LED. The higher AQY when using an LED could be due to the excitation with higher energies above the band gap of the CdS shell. Using the full solar spectrum also excitation only in the CdSe core can be observed which would lead to a less efficient hydrogen production with this wavelength.

The 24 h measurements on the different systems we observed that the CdSe/CdS NR-based hydrogel in combination with the Na_2S/Na_2SO_3 hole scavenger is the most effective system for photocatalytic hydrogen evolution. Therefore, this system was used to investigate the longevity of the gel network as well as the hole scavenger and their effect on the photocatalytic activity in long-term measurements (5 days, **Figure 4**). These measurements were performed in two different variants: I) The hole scavenger in the hydrogel is exchanged every 24 h and the reaction vessel is flushed with nitrogen. II) The hole scavenger is not exchanged and only the reaction vessel is flushed with nitrogen every 24 h. The measurement of the photocatalytic activity over days (Figure 4A) shows that the hydrogels have a constant hydrogen production after 2 days when the hole scavenger solution is exchanged frequently. Without exchange of the hole scavenger solution, the hydrogen production decreases constantly, which is attributed to the consumption of the hole scavenger. Furthermore, it is needed to ensure that the difference between the CdSe/CdS NC solutions and the CdSe/CdS NC-based hydrogels is not only due to the uncontrolled aggregation of the NCs in the Na_2S/Na_2SO_3 hole scavenger solution. Therefore, control experiments under stirring with both a NC solution and a hydrogel have been performed. Stirring can increase the hydrogen production rate for both the NC solution and the hydrogel. However, the stirred NCs still showed a lower hydrogen production rate than the hydrogel without stirring.

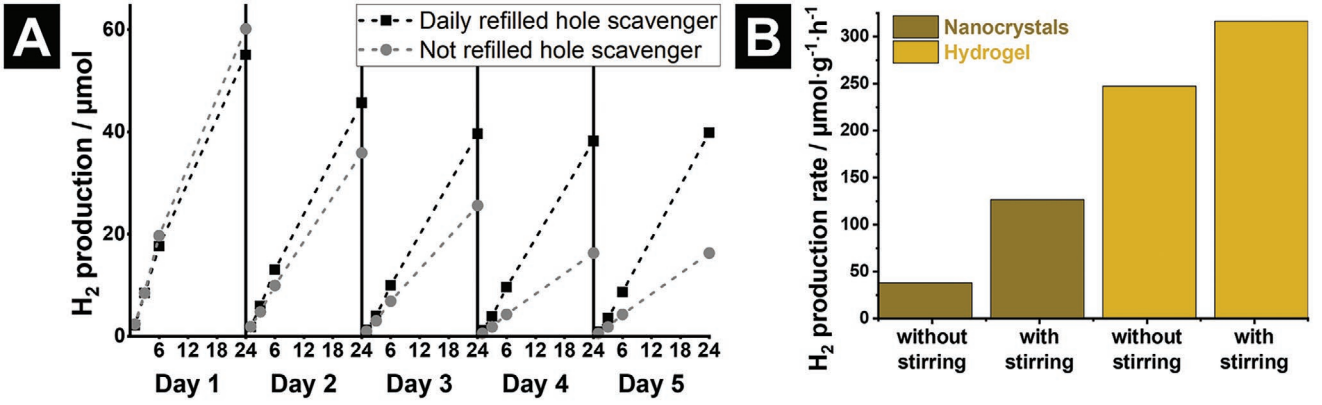

Figure 4. A) Long-term measurements (5 days) on CdSe/CdS NR-based hydrogels show the stability of the photocatalyst and the Na_2S/Na_2SO_3 hole scavenger. After 24 h in one sample (black squares) the hole scavenger solution has been exchanged and the measurement cell has been flushed with nitrogen. The other sample (grey circles) has been flushed with nitrogen without exchanging the hole scavenger solution. The dashed line is used to better visualize the course of the hydrogen production. B) Hydrogen production of NCs in solution and hydrogels with and without stirring, respectively. As hole scavenger solution a mixture of sulfide/sulfite (Na_2S/Na_2SO_3) has been used.

In summary, hydrogen production measurements on CdSe QD, CdS NR, and CdSe/CdS NR-based NC solutions as well as their hydrogels showed up to five times higher hydrogen production rate when using the hydrogel instead of nanocrystal in solution. As hole scavenger a 0.1 M solution of Na_2S/Na_2SO_3 has been the most efficient for all three semiconductor systems. In the following, the differences between the nanocrystals in solution and the hydrogel will be discussed and described using the CdSe/CdS NR-based system as an example, which led to the increased photocatalytic activity.

2.3. Photocatalysis Differences between Ligand-Stabilized Nanocrystals and Hydrogels

Possible reasons for the significantly higher hydrogen production rate of the hydrogels compared to the ligand-stabilized NCs in solution when using sulfite/sulfide as hole scavenger are discussed using CdSe/CdS NRs and their corresponding hydrogel as an example. The proposed mechanism is visualized in **Figure 5**, respectively.

In general, to obtain colloidally stable nanocrystals in solution, their surface is covered with stabilizing ligands, here mercaptopropionic acid (MPA), that can lead to more difficult surface accessibility for the photocatalysis reaction. The MPA ligands used here ensure the colloidal stability and additionally induce hole trap states which influence the charge carrier dynamics.[22] In order to synthesize gels from these nanoparticles, by using a 0.35 wt% H_2O_2 solution to destabilize a ligand-stabilized NC solution, the thiol ligands are oxidized and removed from the NC surface.[30,31] Controlled removal of the ligands, that is, very low concentration of the oxidizing agent, leads to the formation of the porous hydrogel structures shown. In this way, a high surface-to-volume ratio in the hydrogels is retained (Figure S3, Supporting Information), which would, for example, not be the case in compact NC agglomerates. Furthermore, without the ligand shell around the semiconductor NCs, the catalytically active surface is directly accessible for the hydrogen production without steric hindrance from the ligands. Additionally, removal of the thiol ligands leads to free Cd surface atoms, which could enable better interaction of the hole scavenger with excited charge carriers, especially in the 0.1 M Na_2S/Na_2SO_3 solution.

To investigate the differences on the surface of the ligand-stabilized NCs and their hydrogels, XPS measurements were performed (Figure 5B,E). Especially, the S 2p orbital gives a deep insight into the situation at the surface of the semiconductor materials. Figure 5B shows the XPS spectrum of the CdSe/CdS NRs of the S 2p orbital region with the fitted components of the ligand-stabilized NCs dropped on the silicon wafer. The spectrum had to be fitted with five components to achieve a standard deviation close to one. Two components (dark and light orange) can be attributed to the S $2p_{1/2}$ and S $2p_{3/2}$ of sulfur bound in CdS. Two additional components (dark and light blue; for the S $2p_{1/2}$ and S $2p_{3/2}$) are needed to describe the sulfur in the MPA ligand which leads to a shift compared to the sulfur bound in CdS. The fifth component (green) is due to the Se 2p of the CdSe core. The Se 2p binding energy is in

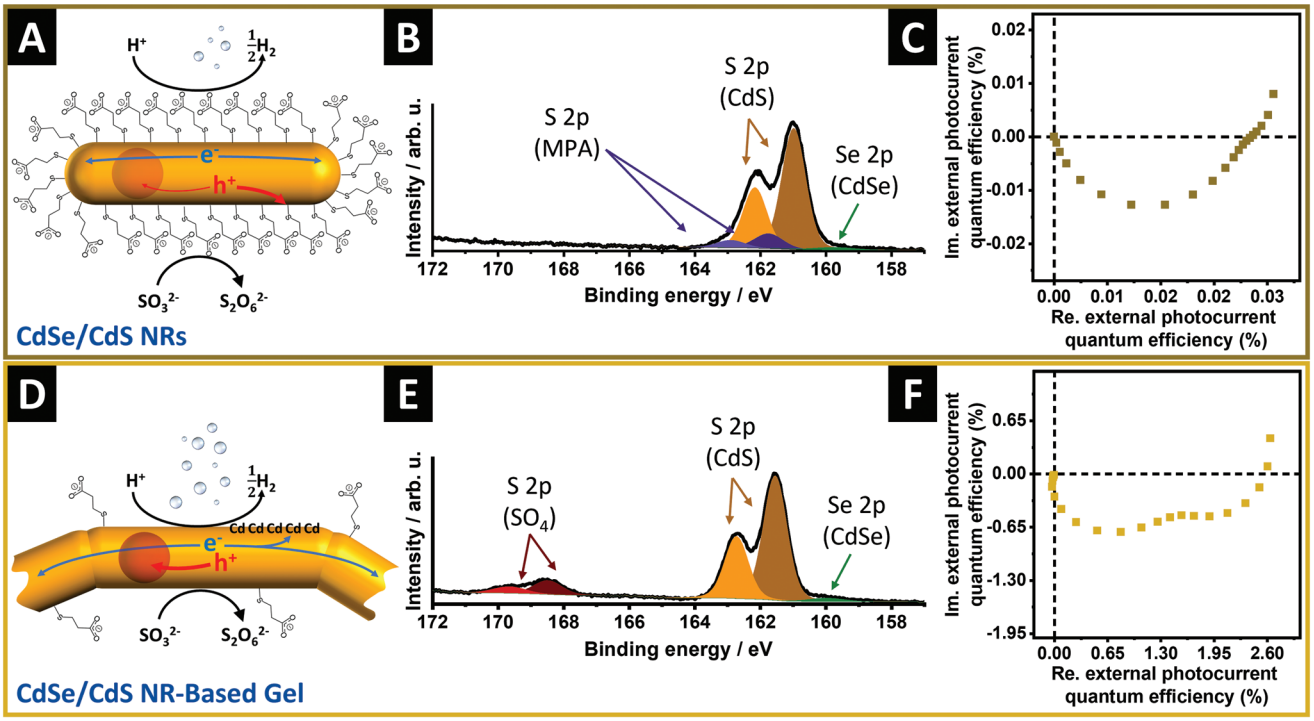

Figure 5. Schematic illustration of the surface and the charge carrier movements in A) CdSe/CdS ligand-stabilized NRs and D) CdSe/CdS NR-based hydrogels. CdCdCdCd represents unsaturated Cd surface atoms due to removed thiol ligands. XPS spectra of the S 2p region showing the differences between B) CdSe/CdS ligand-stabilized NRs and E) CdSe/CdS NR-based hydrogels. Nyquist plots of IMPS measurements of C) CdSe/CdS ligand-stabilized NRs showing one semicircle and Nyquist plots of a F) CdSe/CdS NR-based rehydrated xerogel showing two semicircles.

the same region. Due to the low intensity in the XPS spectrum, only one component is shown for the Se $2p_{3/2}$ state.

A difference can be observed in the XPS spectrum of the S 2p region of the CdSe/CdS NR-based hydrogel which is shown in Figure 5E. Here, the main peaks can be fitted with only three components to achieve a standard deviation close to one, compared to five components required in the ligand-stabilized NC samples. Two components (dark and light orange) can again be attributed to the S $2p_{1/2}$ and S $2p_{3/2}$ of sulfur bound in CdS. The third component (green) with a very low intensity is due to the Se$2p_{3/2}$ bound in the CdSe core. Compared to the pure NC solutions, the components for the sulfur bound in MPA are not needed here, indicating significantly less ligands on the surface of the hydrogels than on the colloidal nanoparticles. In the hydrogel sample there is also a signal with two components (dark and light red) which is shifted to higher binding energies. By comparing the signal position with literature values, this signal can be assigned to the S $2p_{1/2}$ and S $2p_{3/2}$ of sulfur bound in sulfate.[48] During the oxidation of the ligands by the oxidizing agent H_2O_2, the CdS surface is also partially oxidized to sulfate. The presence of sulfate groups on the surface of CdS after treatment with H_2O_2 was previously described by Zhang et al.[48] They also showed that the sulfate ions on the surface can have a positive effect on the catalytic activity due to the preferential bonding of hydrogen atoms on the surface sulfate ions. Furthermore, the Cd3d XPS region gives more evidence for the results discussed with the S 2p and Se 2p regions. The spectra are shown in Figure S8, Supporting Information, and are discussed more deeply in the Supporting Information.

In addition to the changes in surface accessibility and surface modification of the hydrogel, which lead to an increase of the catalytic activity, the charge carrier properties also change. As described earlier, the CdSe/CdS NRs exhibit a quasi-type-II band structure in which the electron can be delocalized over the entire NR while the hole is localized in the CdSe core region. Due to the gelation, the individual NC building blocks are crystalline bound, which results in an extension of the band structure beyond a NC.[31,32,34] The changes in charge carrier properties due to the gelation and the change in the band structure can be described using the optical properties (see Supporting Information). As known from literature, ligands with thiol end groups generate hole trap states at the NC surface. During the gelation process, the removal of the thiol ligands from the surface leads to a reduction of hole trap states on the surface of the semiconductors. Thus, the excited holes are located more probably in the CdSe core, which improves the charge carrier separation and extends the lifetime of the excited charge carriers. Micheel et al. discussed this using the PLQY differences when exciting in the CdSe core and the CdS nanorod, respectively. The PLQY measurements of the semiconductor nanocrystals in solution and their respective hydrogels indicate an improved hole localization in the CdSe core in case of hydrogels.[22,24] Thus, a more pronounced charge carrier separation in the hydrogel compared to the nanocrystals in solution occurs. Since more than one hole in the CdSe core leads to sub-picosecond auger-mediated hole trapping,[48,49] there is a higher probability to have two accessible holes very close to each other in the gel network due to close CdSe cores within the network. This would be beneficial for the whole two step oxidation of the hole scavenger. In the NC solution in contrast two holes have to be more probable from two different NCs which possibly lead to a less efficient hole scavenging process. The excited electron in the interconnected hydrogel can have two different pathways, which both would lead to an extension of the lifetime of the excited charge carriers. First, the electron delocalization in the hydrogel is not limited to the nanocrystal building blocks due to the interconnection of the individual building blocks, so that the charge carrier separation is superior compared to the nanocrystals in solution.[31,32,50] On the other hand, removal of the thiol ligands might lead to free cadmium atoms on the surface of the semiconductor, which are known to act as electron trap states.[22] Both processes would lead to an extension of the lifetime of the excited charge carriers, which is beneficial for the use of the charge carriers for further catalytic reactions. To demonstrate the differences in charge carrier mobility between ligand-stabilized NCs and NC-based gel structures, and to show the ability of the electrons to be located beyond one NC building block, IMPS measurements (Figure 5C,F) were performed. During the IMPS experiments, the on–off frequency of the LED is varied (here from 10 kHz to 1 Hz) and the photocurrent response of the system is recorded.[51] Thus, it is possible to distinguish between charge transfer processes that occur on different time scales, provided their rate constant differ by at least one order of magnitude.[52] A sub-monolayer of CdSe/CdS NRs results in only one semicircle in the Nyquist plots of the IMPS measurements (Figure 5C), which is related to the fast diffusion from electrons from the NRs to the electrode. However, when using CdSe/CdS NR-based xerogels, a second semicircle in the spectrum appears in addition to the first semicircle in the frequency range of 100 to 1 Hz. The second semicircle results from charge carriers which are transported through the gel network and contribute to the measured photocurrent at a longer time scale.[32,34,53,54] The appearance of the second semicircle illustrates the charge carrier mobility in the CdSe/CdS NR-based gel structure compared to non-gelated NCs.

In summary, the higher photocatalytic activity of the NC-based hydrogels compared to the NCs in solution could be explained by optical, XPS, and electrochemical measurements shown above. Removal of the ligands during the oxidative destabilization with H_2O_2 leads to an accessible semiconductor surface without the obstacle of organic ligands. These ligands additionally form hole trap states that reduce the charge carrier separation, so that their absence possibly results in a better charge carrier separation and longer charge carrier lifetimes. In addition to the influence of surface properties, the interconnection of the NCs in the hydrogels enables charge delocalization beyond one NC building block and thus also extends the charge carrier lifetimes. Longer charge carrier lifetimes make the photocatalytic reaction more probable leading to more efficient photocatalysts. Furthermore, the controlled destabilization and hydrogel formation ensures a high surface area which would not be the case by an uncontrolled agglomeration which can be observed using the nanocrystals in solution. As shown above the explanation of the interestingly higher hydrogen production rates using a hydrogel is off several factors. The differentiation of which factor has how many of an impact could not be determined.

3. Conclusion

In the present work, we demonstrate that nanocrystal-based gel networks are of interest for photocatalysis. The photocatalytic hydrogen production of NC-based hydrogels prepared from CdSe QDs, CdS NRs, and CdSe/CdS dot-in-rod NRs was investigated, and the results were compared to those of the pure NCs in solution. Among these semiconductor materials, the efficient charge carrier separation in the CdSe/CdS NRs favored the utilization of charge carriers for the photocatalytic reaction. NC-based hydrogels generally showed five times higher hydrogen production rates compared to their ligand-stabilized NC solutions. Controlled destabilization of the NC solution with a 0.35 wt% H_2O_2 solution as oxidation agent removes the ligands from the nanocrystal surface and leads to a highly porous, self-supporting 3D network. This enables an accessible catalytic surface without a ligand shell, resulting in reduced hole trapping and an extended charge carrier lifetime. In addition to the altered surface properties, the electronic properties in hydrogels differ from those of the NCs in solution. Network formation efficiently separates charge carriers by delocalizing electrons beyond one NC building block, also leading to a longer charge carrier lifetime and a more probable catalytic reaction. It has been shown, that advances in the NC synthesis and controlled destabilization of these ligand-stabilized NC solutions into highly porous gel structures create photocatalytic materials with enhanced photocatalytic activity and a better applicability. The gained knowledge about the photocatalytic behavior of nanocrystal-based hydrogels can further be used to investigate more efficient materials for the photocatalytic hydrogen production.

4. Experimental Section

Chemicals: All chemicals used for the syntheses were used as purchased without any further purification. Cadmium oxide (CdO, 99.998%) and elemental selenium (200 mesh, 99.999%) were supplied by Alfa Aesar. Tri-*n*-octylphosphine oxide (TOPO, 99%), elemental sulfur (99.98%), 1-octadecene (ODE, 90%), 3-mercaptopropionic acid (MPA, ≥99%), 2-propanol (≥99.8%), and chloroform (≥99.5%), were purchased from Sigma-Aldrich. Potassium hydroxide (KOH, >85%), *n*-hexane (≥99%), acetone (99.5%), hydrogen peroxide (H_2O_2, 35 w/w%), toluene (≥99.7%), and MeOH (≥99.8%) were purchased from Honeywell. Tri-*n*-octylphosphine (TOP, 97%) was purchased from ABCR. Elemental tellurium (60 mesh, 99.999%), octadecylphosphonic acid (ODPA, 99.0%), and hexylphosphonic acid (HPA, 99%) were obtained from Roth, Fisher Scientific and PCI, respectively. Ultrapure water with a resistivity of 18.2 MΩ cm was used for aqueous solutions.

Synthesis of CdSe Quantum Dots: The synthesis of the CdSe QDs was adapted from the method of Carbone et al. with certain modifications.[11] In a three-neck flask CdO (0.12 g, 0.93 mmol), TOPO (6.0 g, 15.52 mmol), and ODPA (0.56 g, 1.67 mmol) were degassed under vacuum at 150 °C for 50 min. Under an argon atmosphere, the flask was heated to 300 °C until all CdO was dissolved completely. TOP (3.6 mL) was added, and the temperature was raised to 380 °C. The growth of the CdSe QDs was initiated with the addition of elemental selenium (0.116 g, 1.47 mmol) dissolved in TOP (3.6 mL). After 4 min, the growth was stopped by the addition of ODE (6 mL) and the flask was cooled down quickly using an airflow. Twice, the QDs were precipitated with methanol (5 mL), centrifuged (3775 RCF, 10 min), and redispersed in toluene (5 mL). The size of the nanocrystals and the concentration of the QD solution were determined by the position and the optical density (OD) of the first excitation maximum in an extinction spectrum.[56]

Synthesis of CdS Seeds: CdS seeds were synthesized according to the method of Carbone et al. with certain modifications.[11] For a fourfold scaled synthesis mixture CdO (0.3 g, 2.34 mmol), TOPO (9.9 g, 25.60 mmol), and ODPA (1.81 g, 5.41 mmol) were mixed in a 50 mL three-neck flask, heated up to 150 °C under vacuum, and degassed for 1 h. Subsequently, the solution was heated up to 320 °C under an argon atmosphere followed by the injection of TBP (9.12 mL) consisting $(TMS)_2S$ (0.6 mL). The synthesis was held at 250 °C for 7 min, followed by cooling down to room temperature. At 70 °C 5 mL toluene was added, and the seeds were precipitated by the addition of 10 mL methanol and centrifuged (3775 RCF, 10 min). The CdS seeds were purified twice with a mixture of methanol/toluene (5 mL each) and stored in 1.5 mL toluene.

Synthesis of CdS Nanorods and CdSe/CdS Nanorods: In a modified synthesis of Carbone et al., CdO (0.18 g, 1.4 mmol), TOPO (9.0 g, 23.28 mmol), ODPA (0.84 g, 2.51 mmol), and HPA (0.24 g, 2.07 mmol) were mixed and degassed under vacuum at 150 °C for 1 h.[11] After dissolving the CdO completely at 300 °C under an argon atmosphere, TOP (5.6 mL) was added and the temperature was increased to 380 °C. Once the temperature was reached, the growth of the NRs was initiated by a quick injection of sulfur (0.39 g) dissolved in TOP (5.4 mL) mixed with the previously synthesized CdSe or CdS QDs (concentration of quantum dots in TOP was always 400 µM). After 8 min of reaction, the solution was cooled down by an airflow. At 70 °C, toluene (7 mL) was added and after further cooling (down to ≈30 °C) the particles were precipitated with 10 mL methanol centrifuged (3775 RCF, 10 min). Afterward, the particles have been washed twice with a mixture of methanol/toluene (5 mL each) and redispersed in toluene (2 mL).

Phase Transfer: The method of phase transfer of Kodanek et al. was adapted.[57,58] The nanoparticle solutions were precipitated with methanol, centrifuged and redispersed in 10 mL hexane. The cadmium concentration in the hexane solution was ≈2 mg mL^{-1}. After the addition of a 0.1 M KOH solution in methanol (10 mL) and MPA (0.25 mL) the mixture was shaken for at least 5 h. The methanolic phase with the nanoparticles was separated and centrifuged (3775 RCF, 10 min). After redispersion in a 0.01 M KOH solution in water, the particles were washed with acetone, centrifuged, and finally redispersed in Millipore water.

Assembly to Hydrogels and Transfer to Aerogels: To destabilize the ligand-stabilized nanoparticles by oxidizing the ligands with H_2O_2, the aqueous nanoparticle solution (with a Cd concentration of 3.6 g L^{-1} determined by AAS) was mixed with a H_2O_2 solution (0.35 wt%, 93.75 µL mL^{-1} nanoparticle solution) in an Eppendorf tube or in the photocatalytic glass cells followed by shaking and placing it in an oven at 80 °C for 3 min. Afterward, the solution was stored in the dark overnight. After hydrogelation, ten washing steps over 1 day with Millipore water (2–5 mL for each step) were applied to remove the excess of the destabilizing agent and other by-products. Therefore, 3 mL of the supernatant above the hydrogel has been removed with a pipette and 3 mL fresh Millipore water was carefully added with a pipette. For the BET and SEM measurements, the water was exchanged to dry acetone by washing the gel with mixtures of water and acetone and afterward with pure acetone and anhydrous acetone. To obtain aerogels, the acetogels were dried in a critical point dryer (Quorum Technologies, E3100) using supercritical CO_2. The whole procedure is described in more detail in the previous paper.[31]

Preparation of Xerogel ITO Electrodes: For the photoelectrochemical measurements ITO electrodes were coated with an ambiently dried hydrogel (xerogel). Before coating the electrodes with nanocrystals and nanocrystal-based gel structures, the ITO-coated glass substrates (VisionTek Ltd., 12 $ohms^{-2}$, size of 1.5 cm × 3 cm) were cleaned and activated. For cleaning the glass substrates were rinsed with acetone, 2-propanol, and Millipore water. The activation afterward was performed with a solution of NH_4OH and H_2O_2 (10 mL 25% NH_4OH, 10 mL 35% H_2O_2) in water (60 mL) for 2 h at 70 °C. After washing with water in the next step, the ITO surface was functionalized with 1 vol% MPTMS in toluene for 2 h at 70 °C and have been rinsed with toluene afterward. For NC and NC-based gel coating, a specific area of mold was prepared using a plastic cuvette glued on the ITO substrate with a silicone sealing

paste. The aqueous nanocrystal solution (300 µL) was filled into the glued cuvette and the destabilization was applied as described above using H_2O_2. After the washing steps (ten times with 1 mL Millipore water as described above), the closed hydrogels were stored for 3–4 days. The xerogel was formed by drying the hydrogel under ambient conditions (2 days).

Photocatalysis Measurements: The photocatalysis measurements were performed in Duran glass cells which are shown in Figure S6, Supporting Information. The hydrogels were synthesized inside the cells according to the description above. Before the irradiation with a 300 W xenon lamp (QuantumDesign LSH302) equipped with an AM 1.5 G filter (QuantumDesign solar simulator LS0308), the hydrogels were washed five times with the used hole scavenger solution. To measure the hydrogen production, aliquots (100 µL) were taken with a gas syringe. The aliquots were measured using a GC (Agilent GC 8860) equipped with an Agilent HP-PLOT Molesieve 30 m × 0.320 mm × 25 µm Column and a thermal conductivity detector detector. To calculate the hydrogen production rate, the following equation was used

$$n_{H_2} = \frac{A_{H_2}}{A_{N_2}} \times \text{GC Factor} \times \frac{V_{Gas} p}{RT} \quad (1)$$

$$H_2 \text{ production rate} = \frac{n_{H_2}}{m_{Cd} t} \quad (2)$$

A is the area of the measured peak of hydrogen or nitrogen in the GC. The GC Factor is the ratio of the sensitivity of the thermal conductivity detector regarding hydrogen and nitrogen. The factor was determined with calibration measurements.

The AQY has been calculated using the following equations[59]

$$\text{AQY} = \frac{\text{reacted electrons}}{\text{incident light}} = \frac{2 \times n(H_2)}{n(\text{photons})} = \frac{2 \times n(H_2)}{\frac{I_{inc}}{E_\lambda \times N_A}} = \frac{2 \times n(H_2)}{\frac{I_{inc} \times \lambda}{h \times c \times N_A}} \quad (3)$$

$$I_{inc} = I_0 \times F_A = I_0 \times \frac{\text{absorbed light}}{\text{incoming light}} = I_0 \times \frac{\int_{\lambda_1}^{\lambda_2} I \times (1 - 10^A) \times d\lambda}{\int_{\lambda_1}^{\lambda_2} I \times d\lambda} \quad (4)$$

λ has been assumed to be the wavelength of the energy of the band gap when calculating the AQY with the xenon lamp and the AM1.5 G filter, and λ was set to the wavelength of the LED when calculating the AQY using the LED. The absorbed light and the incoming light were measured using a Thorlabs PM100D power meter with a S121C photodiode (400–1100 nm, 500 mW, d = 9.5 mm). Absorbed light (measured in mW) was determined with the sample in front of the photodiode (absorbed light = incoming light − transmitted light) and incoming light without the sample.

Long-term measurements over days were performed with an Atlas Suntest CPS+ operated at 650 W m^{-2}. The photocatalysis cells were placed in the device with a tilt of 45°. The measurement cells were flushed every 24 h with nitrogen (10 min with two needles; one for the inlet and one for the outlet).

Optical Characterization: Extinction spectra of nanoparticle solutions were performed with a Jasco V-750 spectrometer. Absorption spectra of the nanoparticle solutions and hydrogels were measured in a central position with an Agilent CARY 5000, which was equipped with a Diffuse Reflectance Accessory. The photoluminescence quantum yields were measured with a Quanta-φ integrating sphere coupled to a Horiba Dual-FL spectrofluorometer. Photoluminescence emission and lifetime measurements were conducted in an Edinburgh Instruments FLS 1000 spectrofluorometer using an Edinburgh Instruments EPL 445 pulsed laser (445.1 nm) for excitation of time-resolved measurements. Measurements of nanoparticle solutions, as well as hydrogels, were performed in Hellma Analytic quartz cuvettes.

Structural Characterization: TEM measurements were performed with an FEI Tecnai G2 F20 TMP (operated at 200 kV). Samples were prepared on copper grids which were covered with a carbon layer (Quantifoil). For preparation, hydrogels and colloidal nanocrystal solutions were dropped on the grid. After drying the grids were ready for the measurement in the TEM.

A JEOL JSM-6700F which was operated at 2 kV was used to measure the SEM of the aerogels. For the sample preparation, parts of the aerogel were placed on a conductive carbon.

XPS measurements were conducted using a VersaProbe III from Physical Electronics (ULVAC-PHI) with an AL Kα source at pass energy of 27 eV. Every spectrum was calibrated to the highest intensity of the C 1s peak of each sample. XPS samples were prepared by drop casting 10 µL NC solution as well as hydrogel sample on a Si wafer.

Physisorption Measurements: Argon physisorption was measured with a Micromeritics 3Flex instrument at 87 K. Prior to physisorption measurements, the samples (≈2 mg) were degassed under vacuum at 25 °C for 24 h. Surface areas were estimated by applying the BET equation.

Photoelectrochemical measurements: Measurements were performed in an electrochemical cell which was described by Miethe et al. and is shown in Figure S9, Supporting Information.[52] In the intensity modulated photocurrent spectroscopy, the current response of the electrochemical cell was measured while applying light pulses with various frequencies between 10 kHz and 1 Hz. Hereby, the value of the photocurrent and the phase shift between the sinusoidal light pulses and the sinusoidal current signal were measured. To detect the signal a lock-in amplifier controlled the sinusoidal light pulses with a specific frequency and detects the incoming photocurrent. A lock-in amplifier was necessary because a potentiostat in general was not able to measure the appearing small currents in the range of µA where the noise of the system was larger than the signal itself. As electrolyte, a 0.5 M Na_2SO_3 solution at pH 9 was used. The applied bias potential was measured against a Ag/AgCl reference electrode (3 M NaCl, purchased from BASi). A PE 1542 DC power supply from PHILIPS powered the LED (0.5 mW, λ = 472 nm) and a 7270 DSP lock-in amplifier from AMETEK gave the sinusoidal signal to the LED and detected the current signal from the measurement cell. The bias potential was controlled by the Modulab XM from AMETEK.

Measuring the linear sweep voltammetry includes a scan from low to higher bias potentials over a fixed time range. In the experiments, the voltage was applied from –0.6 up to 0.3 V with a slope of 0.2 V min^{-1}. Before starting the measurement, a constant potential was applied for 30 s at the starting voltage of –0.6 V to reach an equilibrium state for the whole system. During the linear sweep voltammetry, the LED was turned on and off periodically with a frequency of 40 mHz. This corresponds to a time period of 12.5 s of irradiation and 12.5 s of darkness. To apply the voltage the potentiostat Modulab XM from AMETEK was used and the control system for the LED was the arbitrary generator HMF2550 from Rohde and Schwarz.

Supporting Information

Supporting Information is available from the Wiley Online Library or from the author.

Acknowledgements

J.S. and F.L.-W. contributed equally to this work. This work was funded by the German Research Foundation (Deutsche Forschungsgemeinschaft, DFG) with the grant agreement BI 1708/4-1 and under Germany's excellence strategy within the cluster of excellence PhoenixD (EXC 2122, project ID 390833453). The studies performed in the laboratory

"Photoactive nanocomposite materials" were supported by Saint-Petersburg State University (ID: 73032813). R.T.G. is thankful for financial support from the Hannover School for Nanotechnology (hsn). Moreover, the authors thank Armin Feldhoff and Jürgen Caro for providing the SEM and XRD facility, and thank the Laboratory of Nano and Quantum Engineering for access to TEM.

Open access funding enabled and organized by Projekt DEAL.

Conflict of Interest

The authors declare no conflict of interest.

Data Availability Statement

The data that support the findings of this study are available from the corresponding author upon reasonable request.

Keywords

charge carrier separation, nanocrystal-based hydrogels, photocatalysis, photocatalytic hydrogen production, self-assembly

Received: December 23, 2022
Revised: February 3, 2023
Published online: February 24, 2023

[1] D. Gielen, F. Boshell, D. Saygin, M. D. Bazilian, N. Wagner, R. Gorini, *Energy Strategy Rev.* **2019**, *24*, 38.
[2] K. C. Christoforidis, P. Fornasiero, *ChemCatChem* **2017**, *9*, 1523.
[3] M. Tahir, S. Tasleem, B. Tahir, *Int. J. Hydrogen Energy* **2020**, *45*, 15985.
[4] H. Zhao, H. Fu, X. Yang, S. Xiong, D. Han, X. An, *Int. J. Hydrogen Energy* **2022**, *47*, 8247.
[5] W.-K. Jo, T. S. Natarajan, *Chem. Eng. J.* **2015**, *281*, 549.
[6] R. Costi, A. E. Saunders, U. Banin, *Angew. Chem., Int. Ed.* **2010**, *49*, 4878.
[7] M. Nasilowski, B. Mahler, E. Lhuillier, S. Ithurria, B. Dubertret, *Chem. Rev.* **2016**, *116*, 10934.
[8] F. Montanarella, M. V. Kovalenko, *ACS Nano* **2022**, *16*, 5085.
[9] A. L. Efros, L. E. Brus, *ACS Nano* **2021**, *15*, 6192.
[10] X. Peng, L. Manna, W. Yang, J. Wickham, E. Scher, A. Kadavanich, A. P. Alivisatos, *Nature* **2000**, *404*, 59.
[11] L. Carbone, C. Nobile, M. de Giorgi, F. della Sala, G. Morello, P. Pompa, M. Hytch, E. Snoeck, A. Fiore, I. R. Franchini, M. Nadasan, A. F. Silvestre, L. Chiodo, S. Kudera, R. Cingolani, R. Krahne, L. Manna, *Nano Lett.* **2007**, *7*, 2942.
[12] D. V. Talapin, R. Koeppe, S. Götzinger, A. Kornowski, J. M. Lupton, A. L. Rogach, O. Benson, J. Feldmann, H. Weller, *Nano Lett.* **2003**, *3*, 1677.
[13] A. Schlosser, R. T. Graf, N. C. Bigall, *Nanoscale Adv.* **2020**, *2*, 4604.
[14] S. Naskar, A. Schlosser, J. F. Miethe, F. Steinbach, A. Feldhoff, N. C. Bigall, *Chem. Mater.* **2015**, *27*, 3159.
[15] M. Berr, A. Vaneski, A. S. Susha, J. Rodríguez-Fernández, M. Döblinger, F. Jäckel, A. L. Rogach, J. Feldmann, *Appl. Phys. Lett.* **2010**, *97*, 093108.
[16] F. Qiu, Z. Han, J. J. Peterson, M. Y. Odoi, K. L. Sowers, T. D. Krauss, *Nano Lett.* **2016**, *16*, 5347.
[17] V. L. Bridewell, R. Alam, C. J. Karwacki, P. V. Kamat, *Chem. Mater.* **2015**, *27*, 5064.
[18] P. Zeng, W.-D. Zhang, *Mol. Catal.* **2021**, *515*, 111856.
[19] L. Amirav, A. P. Alivisatos, *J. Phys. Chem. Lett.* **2010**, *1*, 1051.
[20] P. Kalisman, L. Houben, E. Aronovitch, Y. Kauffmann, M. Bar-Sadan, L. Amirav, *J. Mater. Chem. A* **2015**, *3*, 19679.
[21] Y. Nakibli, L. Amirav, *Chem. Mater.* **2016**, *28*, 4524.
[22] M. Micheel, B. Liu, M. Wächtler, *Catalysts* **2020**, *10*, 1143.
[23] R. Abargues, J. Navarro, P. J. Rodríguez-Cantó, A. Maulu, J. F. Sánchez-Royo, J. P. Martínez-Pastor, *Nanoscale* **2019**, *11*, 1978.
[24] Y. Ben-Shahar, F. Scotognella, N. Waiskopf, I. Kriegel, S. Dal Conte, G. Cerullo, U. Banin, *Small* **2015**, *11*, 462.
[25] A. Eychmüller, *J. Phys. Chem. C* **2022**, *126*, 19011.
[26] C. Ziegler, A. Wolf, W. Liu, A.-K. Herrmann, N. Gaponik, A. Eychmüller, *Angew. Chem., Int. Ed.* **2017**, *56*, 13200.
[27] P. Rusch, D. Zámbó, N. C. Bigall, *Acc. Chem. Res.* **2020**, *53*, 2414.
[28] F. Rechberger, M. Niederberger, *Nanoscale Horiz.* **2017**, *2*, 6.
[29] I. U. Arachchige, S. L. Brock, *J. Am. Chem. Soc.* **2006**, *128*, 7964.
[30] J. L. Mohanan, I. U. Arachchige, S. L. Brock, *Science* **2005**, *307*, 397.
[31] S. Sánchez-Paradinas, D. Dorfs, S. Friebe, A. Freytag, A. Wolf, N. C. Bigall, *Adv. Mater.* **2015**, *27*, 6152.
[32] J. F. Miethe, F. Luebkemann, A. Schlosser, D. Dorfs, N. C. Bigall, *Langmuir* **2020**, *36*, 4757.
[33] D. Zámbó, A. Schlosser, P. Rusch, F. Lübkemann, J. Koch, H. Pfnür, N. C. Bigall, *Small* **2020**, *16*, 1906934.
[34] F. Lübkemann, J. F. Miethe, F. Steinbach, P. Rusch, A. Schlosser, D. Zámbó, T. Heinemeyer, D. Natke, D. Zok, D. Dorfs, N. C. Bigall, *Small* **2019**, *15*, 1902186.
[35] L. Korala, J. R. Germain, E. Chen, I. R. Pala, D. Li, S. L. Brock, *Inorg. Chem. Front.* **2017**, *4*, 1451.
[36] S. Brunauer, P. H. Emmett, E. Teller, *J. Am. Chem. Soc.* **1938**, *60*, 309.
[37] P. Rusch, B. Schremmer, C. Strelow, A. Mews, D. Dorfs, N. C. Bigall, *J. Phys. Chem. Lett.* **2019**, *10*, 7804.
[38] F. Lübkemann, P. Rusch, S. Getschmann, B. Schremmer, M. Schäfer, M. Schulz, B. Hoppe, P. Behrens, N. C. Bigall, D. Dorfs, *Nanoscale* **2020**, *12*, 5038.
[39] P. Rusch, B. Schremmer, C. Strelow, A. Mews, D. Dorfs, N. C. Bigall, *J. Phys. Chem. Lett.* **2019**, *10*, 7804.
[40] M. Berr, A. Vaneski, A. S. Susha, J. Rodríguez-Fernández, M. Döblinger, F. Jäckel, A. L. Rogach, J. Feldmann, *Appl. Phys. Lett.* **2010**, *97*, 093108.
[41] Y. Nakibli, Y. Mazal, Y. Dubi, M. Wächtler, L. Amirav, *Nano Lett.* **2018**, *18*, 357.
[42] K. Dong, C. Pezzetta, Q. C. Chen, A. Kaushansky, A. Agosti, G. Bergamini, R. Davidson, L. Amirav, *ChemCatChem* **2022**, *14*, 202200477.
[43] D. Meissner, R. Memming, B. Kastening, D. Bahnemann, *Chem. Phys. Lett.* **1986**, *127*, 419.
[44] J. Schneider, D. W. Bahnemann, *J. Phys. Chem. Lett.* **2013**, *4*, 3479.
[45] M. J. Berr, P. Wagner, S. Fischbach, A. Vaneski, J. Schneider, A. S. Susha, A. L. Rogach, F. Jäckel, J. Feldmann, *Appl. Phys. Lett.* **2012**, *100*, 223903.
[46] Y. J. Tu, D. Njus, H. B. Schlegel, *Org. Biomol. Chem.* **2017**, *15*, 4417.
[47] P. Kalisman, Y. Nakibli, L. Amirav, *Nano Lett.* **2016**, *16*, 1776.
[48] Z. Zhang, M. Wang, H. Zhou, F. Wang, *J. Am. Chem. Soc.* **2021**, *143*, 6533.
[49] S. Dong, S. Pal, J. Lian, Y. Chan, O. V. Prezhdo, Z. H. Loh, *ACS Nano* **2016**, *10*, 9370.
[50] A. Efros, in *Semiconductor Nanocrystals: From Basic Principles to Applications*, (Eds: A. L. Efros, D. J. Lockwood, L. Tsybeskov, Springer US, Boston, MA, **2003**, pp. 52–72.
[51] P. Rusch, F. Lübkemann, H. Borg, J. G. Eckert, D. Dorfs, N. C. Bigall, *J. Chem. Phys.* **2022**, *156*, 234701.
[52] L. M. Peter, J. Li, R. Peat, H. J. Lewerenz, J. Stumper, *Electrochim. Acta* **1990**, *35*, 1657.
[53] J. F. Miethe, F. Lübkemann, J. Poppe, F. Steinbach, D. Dorfs, N. C. Bigall, *ChemElectroChem* **2018**, *5*, 175.
[54] J. Schlenkrich, D. Zámbó, A. Schlosser, P. Rusch, N. C. Bigall, *Adv. Opt. Mater.* **2022**, *10*, 2101712.

[55] A. Schlosser, L. C. Meyer, F. Lübkemann, J. F. Miethe, N. C. Bigall, *Phys. Chem. Chem. Phys.* **2019**, *21*, 9002.
[56] W. W. Yu, L. Qu, W. Guo, X. Peng, *Chem. Mater.* **2004**, *16*, 560.
[57] T. Kodanek, H. M. Banbela, S. Naskar, P. Adel, N. C. Bigall, D. Dorfs, *Nanoscale* **2015**, *7*, 19300.
[58] H. G. Bagaria, E. T. Ada, M. Shamsuzzoha, D. E. Nikles, D. T. Johnson, *Langmuir* **2006**, *22*, 7732.
[59] S. Naskar, F. Lübkemann, S. Hamid, A. Freytag, A. Wolf, J. Koch, I. Ivanova, H. Pfnür, D. Dorfs, D. W. Bahnemann, N. C. Bigall, *Adv. Funct. Mater.* **2017**, *27*, 1604685.